and $\lim_{n\to\infty} \min_i\{S_{in}\}/n = b$ with probability 1. From (20)–(21), $\max_i\{S_{in}\} = S_{0n}$ for all $n > L$, which implies that $a = ph$. If $b = ph$, $\lim_{n\to\infty} S_{in} = ph$ and it can be shown that $ph = \phi_q$. The proof is then completed. Consider now the case $b < ph$. Since $\max_i\{S_{in}\} = S_{0n}$ for all $n > L$, there exists a transition $z(n) \in T_q$, such that $S_{z(n),n} = \min_i\{S_{in}\}$. Since $N_q$ is a strongly connected event graph, $S_{z(n),n} + m_{(z(n),j)} = S_{in}$ for all $i \in T_q$, leading to $\lim_{n\to\infty} S_{in}/n = b$ w.p 1 $\forall\, i \in T_q$. As a result, there exists an integer $L' \geq L$, such that $S_{in}/n < (b+a)/2\ \forall\, i \in T_q$ and $S_{0n}/n > (b+a)/2\ \forall\, n \geq L'$. Under such conditions, (20) becomes $S_{in+1} = \min_{j\in T_q}\{S_{jn} + A_{jn}\tau_n + m_{(j,i)}\}\ \forall\, i \in T_q$, and $\forall\, n \geq L'$. Applying *Theorem 6* to the above recursion leads to $\lim_{n\to\infty} S_{in}/n = \phi_q$ with probability 1 $\forall\, i \in T_q$, which completes the proof.

## REFERENCES


[1] F. Baccelli and J. Mairesse, "Ergodic theorems for stochastic operators and discrete event networks," INRIA, Metz, France, Res. Rep. #2641, 1995.

[2] M. Caramanis and G. Leberopoulos, "Perturbation analysis for the design of flexible manufacturing system flow controllers," *Oper. Res.*, vol. 40, pp. 1107–1125, 1992.

[3] R. David and H. Alla, *Petri Nets and Grafcet: Tools for Modeling of Discrete Event Systems*. London, U.K.: Prentice-Hall, 1992.

[4] A. Haurie, P. L'Ecuyer, and Ch. Van Delft, "Convergence of stochastic approximation coupled with perturbation analysis in a class of manufacturing flow control models," *J. Discrete Event Dynam. Syst., Theory Applicat.*, vol. 4, pp. 87–111, 1994.

[5] C. G. Panayiotou and C. G. Cassandras, "Optimization of Kanban-based manufacturing systems," *Automatica*, vol. 35, pp. 1521–1533, 1999.

[6] E. L. Plambeck, B.-R. Fu, S. M. Robinson, and R. Suri, "Sample-path optimization of convex stochastic performance functions," *Math. Programming*, vol. 75, pp. 137–176, 1996.

[7] S. M. Robinson, "Analysis of sample-path optimization," *Math. Oper. Res.*, vol. 21, pp. 513–528, 1996.

[8] R. Suri and B.-R. Fu, "On using continuous flow lines to model discrete production lines," *J. Discrete Event Dynam. Syst., Theory Applicat.*, vol. 4, pp. 127–169, 1994.

[9] K. S. Trivedi and V. G. Kulkarni, "FSPN: Fluid stochastic Petri nets," in *Application and Theory of Petri Nets*, M. Ajmone-Marsan, Ed. Berlin, Germany: Springer-Verlag, 1993.

[10] X. Xie, "Evaluation and optimization of two-stage continuous transfer lines subject to time-dependent failures," in *Proc. WoDES'98*, Cagliari, Sardinia, 1998, pp. 112–117.

[11] H. Yan, G. Yin, and S. X. C. Lou, "Using stochastic optimization to determine threshold values for the control of unreliable manufacturing systems," *J. Optim. Theory Appl.*, vol. 83, pp. 511–539, 1994.


# Eclipse II: A New Parallel Mechanism Enabling Continuous 360-Degree Spinning Plus Three-Axis Translational Motions

Jongwon Kim, Jae Chul Hwang, Jin Sung Kim, Cornel C. Iurascu, Frank Chongwoo Park, and Young Man Cho

***Abstract*—This paper presents the Eclipse II, a new six-degrees-of-freedom parallel mechanism, which can be used as a basis for general motion simulators. The Eclipse II is capable of $x$, $y$, and $z$ axes translations, and $a$, $b$, and $c$ axes rotations. In particular, it has the advantage of enabling continuous 360° spinning of the platform. We first describe the computational procedures for the forward and inverse kinematics of the Eclipse II. Next, the complete singularity analysis is presented for the two cases of end-effector singularity and actuator singularity. Finally, two additional actuators are added to the original mechanism to eliminate both types of singularity within the workspace.**

***Index Terms*—Motion simulator, parallel mechanism, singularity analysis, workspace analysis.**

## I. INTRODUCTION

Motion simulators are virtual reality systems that assume the appearance of a real situation by using audiovisual effects and movements of a motion base. Such devices are used for many purposes, e.g., flight and driving simulators, to name only two. The former are used for pilot training by providing the pilot with motions that reflect the state of the aircraft, while the latter reproduce actual driving conditions for vehicle design and human factors studies. Broadly speaking, a motion simulator consists of an auditory system to generate sound, a visual system to display images, and a motion-base system to generate movements as a result of motion cues.

Most current simulators have adopted the Stewart–Gough platform shown in Fig. 1 as the motion base (see [1]–[4] for a survey on parallel mechanisms and list of references). This platform is a six-degrees-of-freedom parallel mechanism that allows both translational and rotational motions. The platform can only tilt as much as $\pm 20^\circ$–$30^\circ$, and large motions, such as the $360^\circ$ overturn, are impossible. That is, the overturn motion of the aircraft or the $360^\circ$ spin of the roller coaster cannot be reproduced by the Stewart–Gough platform.

Some other parallel mechanisms that display relatively large translational or rotational motions are the Delta robot [5] and the spherical parallel mechanism [6], [7]. Yet, the kinematic mobility of these mechanisms is not six, and they are used either for positioning or orienting applications. Closer to the spirit of our design is the redundantly actuated Eclipse I mechanism (see [8] and references cited therein), devised specifically for machining applications. This mechanism has a large workspace and all closed trajectories on five faces of a cube can be traced without breaking contact. Although the spindle can rotate $360^\circ$ around the fixed $z$ axis and tilt concomitantly, the tilting angle of the upper plate does not exceed $90^\circ$ with respect to the vertical. Hence, large overturn motions are impossible.

Manuscript received April 27, 2001; revised December 1, 2001. This paper was recommended for publication by Associate Editor G. Chirikjian and Editor I. Walker upon evaluation of the reviewers' comments. This work was supported in part by the National Research Laboratory on Innovative Parallel Mechanism Platforms and in part by the Brain Korea 21 program, both at Seoul National University.

The authors are with the School of Mechanical and Aerospace Engineering, Seoul National University, Seoul 151-742, Korea (e-mail: jongkim@snu.ac.kr; hjc@rodel.snu.ac.kr; lus@plaza1.snu.ac.kr; kjs@rodel.snu.ac.kr; fcp@plaza.snu.ac.kr; choym@gong.snu.ac.kr).

Publisher Item Identifier S 1042-296X(02)05179-0.

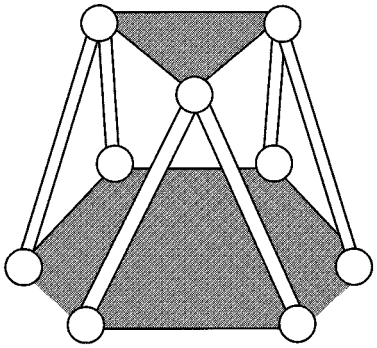

Fig. 1. Structure of Stewart–Gough platform.

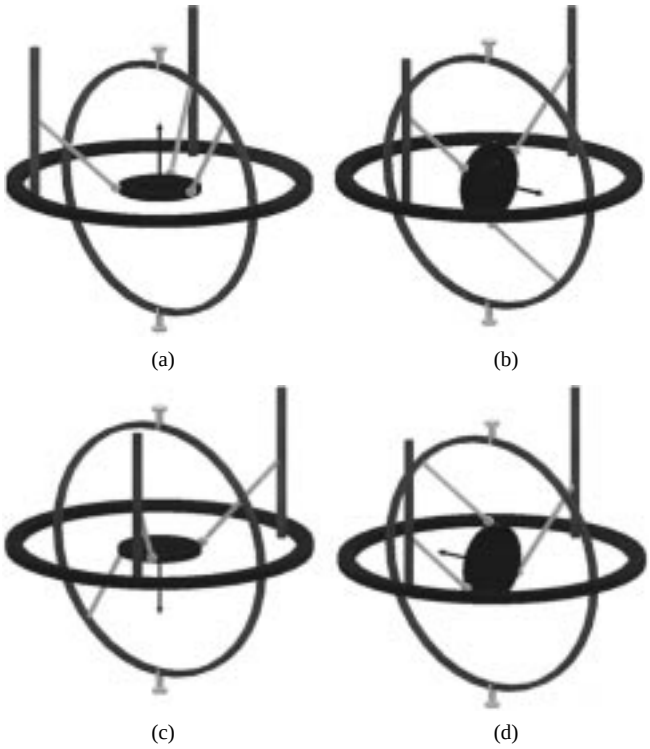


Fig. 2. Eclipse II mechanism and its 360° continuous rotational motions. (a) Rotation angle 0°. (b) Rotation angle 90°. (c) Rotation angle 180°. (d) Rotation angle 270°.

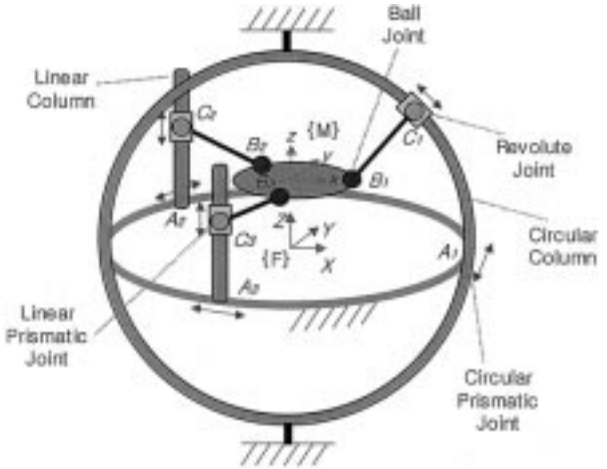


Fig. 3. Architecture of the Eclipse II mechanism.

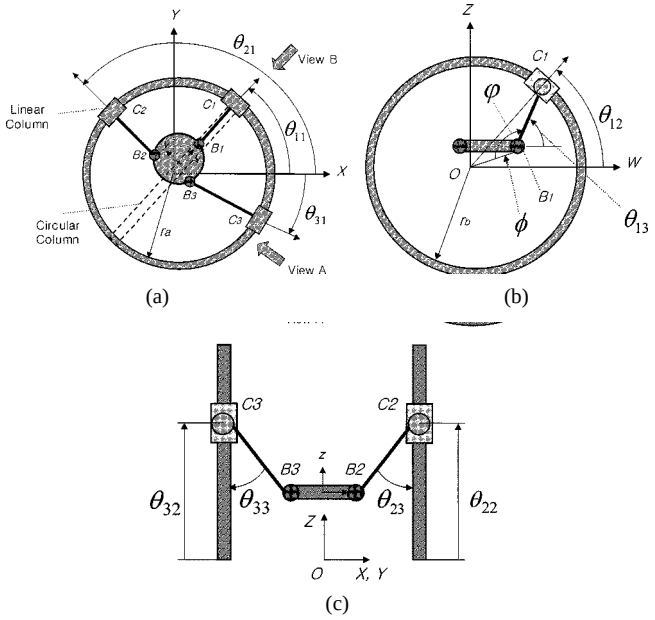


Fig. 4. Coordinate and joint convention. (a) Top view. (b) Side view A. (c) Side view B.

The objective of the present research is to develop a mechanism capable of 360° tilting motion of the platform as well as translational motion. Fig. 2 shows the Eclipse II mechanism and an example of its rotational motion capability. Since there are no limits in the rotational motion, it is possible to design a more realistic and higher fidelity motion simulator.

This paper is organized as follows. In Section II, we describe the kinematic structure of the Eclipse II, including the computational procedures for the forward and inverse kinematics. The singularity analysis and a method for eliminating the singularities are presented in Section III. In Section IV, we describe the workspace analysis and present a structure for maximizing the workspace. Finally, some concluding remarks follow in Section V.

## II. Kinematics of the Eclipse II

This section presents the architecture of the Eclipse II, followed by the procedures describing the inverse and forward kinematics. As shown in Fig. 3, the Eclipse II consists of three PPRS serial subchains that move independently on a fixed circular guide. Here, $P$, $R$, and $S$ denote prismatic, revolute, and spherical joints, respectively. The Eclipse II has six degrees of freedom and six actuated joints. These joints are the three $A$ joints ($P$) along the horizontal circular guide, the $C_2$ and $C_3$ joints ($P$) on the vertical columns, and another $P$ joint ($C_1$) on the vertical circular column. All six actuated joints can be found in Fig. 3, and are indicated by arrows. The connecting links, $C_iB_i$, are attached to the circular and vertical columns, respectively, through revolute joints. The other ends of these links are mounted to the moving platform via three points $B_i$ in Fig. 3, ball-and-socket joints. Mounting one circular column and two linear columns on the circular guide results in the Eclipse II having a large orientation workspace. Thus, the platform can rotate 360° continuously about the $y$ axis in the moving frame $\{M\}$ (center of the moving platform), and the $z$ axis in the fixed frame $\{F\}$ (center of the fixed horizontal track) as shown in Fig. 3. Coordinates and joint convention of the Eclipse II are described in Fig. 4. The kinematic parameters of the mechanism are the fixed circular guide radius, $r_a$, the circular column radius, $r_b$, the radius of the moving platform, $r$, the length of the connecting $C_iB_i$ links, $Li$, and $d$, the distance between the spherical joints on the upper platform. The joint values are referred to as $\theta_{ij}$, where $i$ stands generally for the column index and

$j$ for the joint level (1 for the fixed circular guide, 2 for the circular and linear columns, and 3 for the revolute on the same columns). For instance, $\theta_{32}$ refers to the prismatic joint on the third linear column.

### A. Inverse Kinematics

The problem of inverse kinematics is to determine the values of the actuated joints from the position and orientation of the moving frame $\{M\}$ attached to the moving platform. For the Eclipse II mechanism, the inverse kinematics can be solved by successively solving the inverse kinematics of each subchain. The algorithm for solving the inverse kinematics is

1) Given the position $\vec{p}$ and orientation $R$ of the moving platform in the fixed $\{F\}$ frame, find the Cartesian position of the spherical joints

$$\overrightarrow{b_i} = R^M \overrightarrow{b_i} + \overrightarrow{p} \tag{1}$$

where ${}^M\overrightarrow{b_i}$ is the vector of the $i$th spherical joint expressed in the moving frame coordinate. $R$, $\vec{p}$, and $\vec{b}_i$ are all expressed in the fixed frame coordinates.

2) The circular prismatic joint values ($A_i$) are calculated from the positions of the spherical joints as follows:

$$\theta_{i1} = \arctan 2(b_{iy},\, b_{ix}) \tag{2}$$

where $\theta_{i1}$ is the $i$th circular prismatic joint value, and $b_{ix}$ and $b_{ix}$ are the $x$ and $y$ coordinates of $\vec{b}_i$, respectively.

3) Calculate the revolute joint value, $\theta_{13}$ [see Fig. 4(b)], on the vertical circular column

$$\theta_{13} = 180^\circ + \phi - \varphi \tag{3}$$

where

$$\phi = \arcsin\left(\frac{b_{1z}}{\left\|\overrightarrow{b_1}\right\|}\right)$$

$$\phi = \arccos\left(\frac{\left\|\overrightarrow{b_1}\right\|^2 + L_1^2 - r_b^2}{2\cdot\left\|\overrightarrow{b_1}\right\|\cdot L_1}\right).$$

4) Determine the prismatic joint values, $\theta_{12}$, on the vertical circular column

$$\theta_{12} = \arctan 2(a_{1z},\, a_{1w}) \tag{4}$$

where

$$a_{1z} = L_1\cos\theta_{13} + \left\|\overrightarrow{b_1}\right\|\cos\phi$$

$$a_{1w} = L_1\sin\theta_{13} + \left\|\overrightarrow{b_1}\right\|\sin\phi.$$

5) Find the linear prismatic joint values, $\theta_{i2}(i = 2, 3)$, and the position of the revolute joints, $\theta_{i3}(i = 2, 3)$, on the vertical linear columns

$$\theta_{i2} = -d_i + \sqrt{d_i^2 - e_i}\ (i = 2, 3) \tag{5}$$

where

$$\overrightarrow{n} = [\,0 \quad 0 \quad 1\,]^T,\ \vec{a}_i = [\,r_a\cos\theta_{i1} \quad r_a\sin\theta_{i1} \quad 0\,]^T$$

$$d_i = \left(\overrightarrow{a_i} - \overrightarrow{b_i}\right)\cdot\overrightarrow{n},\ e_i = \left\|\overrightarrow{a_i} - \overrightarrow{b_i}\right\|^2 - L_i^2$$

and

$$\theta_{i3} = \arccos\left(\frac{\left(\vec{b}_i - \vec{c}_i\right)\cdot\vec{n}}{\left\|\vec{b}_i - \vec{c}_i\right\|\cdot\|\vec{n}\|}\right). \tag{6}$$

Note that the solution of $\theta_{i3}$ is in the range [0°–180°].

### B. Forward Kinematics

The problem of forward kinematics is to determine the position and orientation of the moving frame given the actuated joint values. Similar to many other parallel mechanisms, the forward kinematics solution is not unique, and finding a closed form solution is a difficult task. If all of the actuated and passive joint values are known, the forward kinematics can be solved from the forward kinematics of each serial subchain. Therefore, the first step in the forward kinematics solution is to numerically determine the passive joint values from the actuated joint values by using the kinematics constraint equations.

The following algorithm solves iteratively the forward kinematic using the Newton–Raphson procedure.

1) The constraint equation between the active and passive joint values is generated from the condition that the distances between the ball-and-socket joints of the moving platform are constant

$$\vec{g}\left(\vec{\theta}_a,\, \vec{\theta}_p\right) = \vec{0} \tag{7}$$

where

$$\vec{g}\left(\vec{\theta}_a,\, \vec{\theta}_p\right) = \begin{bmatrix} \left(\overrightarrow{b_1} - \overrightarrow{b_2}\right)\cdot\left(\overrightarrow{b_1} - \overrightarrow{b_2}\right) - d^2 \\ \left(\overrightarrow{b_2} - \overrightarrow{b_3}\right)\cdot\left(\overrightarrow{b_2} - \overrightarrow{b_3}\right) - d^2 \\ \left(\overrightarrow{b_3} - \overrightarrow{b_1}\right)\cdot\left(\overrightarrow{b_3} - \overrightarrow{b_1}\right) - d^2 \end{bmatrix}$$

$$\overrightarrow{b_i} = \begin{cases} \begin{bmatrix} \cos\theta_{i1}(r_a\cos\theta_{i2} - L_i\cos\theta_{i3}) \\ \sin\theta_{i1}(r_a\cos\theta_{i2} - L_i\cos\theta_{i3}) \\ r_a\sin\theta_{i2} - L_i\sin\theta_{i3} \end{bmatrix}, & i = 1 \\ \begin{bmatrix} \cos\theta_{i1}(r_a - L_i\sin\theta_{i3}) \\ \sin\theta_{i1}(r_a - L_i\sin\theta_{i3}) \\ \theta_{i2} - L_i\cos\theta_{i3} \end{bmatrix}, & i = 2, 3 \end{cases}$$

$$\vec{\theta}_a = [\,\theta_{11} \quad \theta_{12} \quad \theta_{21} \quad \theta_{22} \quad \theta_{31} \quad \theta_{32}\,]^T$$

$$\vec{\theta}_p = [\,\theta_{13} \quad \theta_{23} \quad \theta_{33}\,]^T. \tag{8}$$

2) Given the actuated joint values, find the passive joint values for which the kinematic constraint equation (7) is satisfied. Because analytic differentiation of (7) is quite simple, a numerical approach like the Newton–Raphson method can be easily applied [9], [10].

3) Determine the position and orientation of the moving frame from the forward kinematics equations for each subchain, (8), for the Cartesian coordinates of the spherical joints, and (9) and (10), from the next section, for the position and orientation of the upper platform.

## III. Singularity Analysis

Singularity refers to the configuration in which the number of degrees of freedom of the mechanism increases or reduces instantaneously. Since being close to one of the singularities can limit movement, disable control, or break the mechanism, the singularity analysis is one of the most significant and critical problems in the design and control of parallel mechanisms.

Singularities of parallel mechanisms can be generally classified into two types, end-effector singularity and actuator singularity [4]. For the Eclipse II mechanism, these two types of singularities coexist in the workspace. In this section, the singular configuration of the Eclipse II mechanism and the method for eliminating singularities are described.

The kinematic parameters used for singularity analysis are specified as follows. The radius of the circular guide ($r_a$), circular column ($r_b$), and moving platform ($r$) are, respectively, 1000, 1000, and 300 mm. The lengths of the connecting link in the circular column ($L_1$) and of the connecting links in the linear column ($L_2$, $L_3$) are, respectively, 900 and 870 mm.

### A. End-Effector Singularity

The end-effector singularity is the configuration in which the moving platform of the mechanism loses one or more degrees of freedom of possible motion. In this case, the forward kinematic Jacobian loses rank. For Eclipse II, the algorithm for solving the forward Jacobian is

1) The position of the moving platform $\vec{b}_c$ is the center of an equilateral triangle determined by the three spherical joints

$$\vec{b}_c = \frac{1}{3}\left(\vec{b}_1 + \vec{b}_2 + \vec{b}_3\right). \tag{9}$$

2) The rotational matrix representing the orientation of the moving platform is

$$R = [\, R^x \quad R^y \quad R^z \,] \tag{10}$$

where

$$R^x = \frac{1}{r}\left(\vec{b}_1 - \vec{b}_c\right)$$
$$R^y = \frac{1}{\sqrt{3}r}\left(\vec{b}_2 - \vec{b}_3\right)$$
$$R^z = R^x \times R^y.$$

3) In order to obtain the Jacobian matrix, (9) and (10) are differentiated

$$\begin{bmatrix} v \\ w \end{bmatrix} = J\dot{\theta}, \quad J \in R^{6\times 9}. \tag{11}$$

Elements of the Jacobian, $J$, are

$$J_i = \begin{bmatrix} \frac{1}{3}\frac{\partial \vec{b}_i}{\partial \theta_i} \\ R^z \cdot \frac{\partial R^y}{\partial \theta_i} \\ -R^z \cdot \frac{\partial R^x}{\partial \theta_i} \\ -R^x \cdot \frac{\partial R^y}{\partial \theta_i} \end{bmatrix}, \qquad i = 1, 2, \ldots, 9$$

where $\vec{b}_1 = \vec{b}_4 = \vec{b}_7$, $\vec{b}_2 = \vec{b}_5 = \vec{b}_8$, $\vec{b}_3 = \vec{b}_6 = \vec{b}_9$, $\theta_1 = \theta_{11}$, $\theta_2 = \theta_{21}$, $\theta_3 = \theta_{31}$, $\theta_4 = \theta_{12}$, $\theta_5 = \theta_{22}$, $\theta_6 = \theta_{32}$, $\theta_7 = \theta_{13}$, $\theta_8 = \theta_{23}$, $\theta_9 = \theta_{33}$.

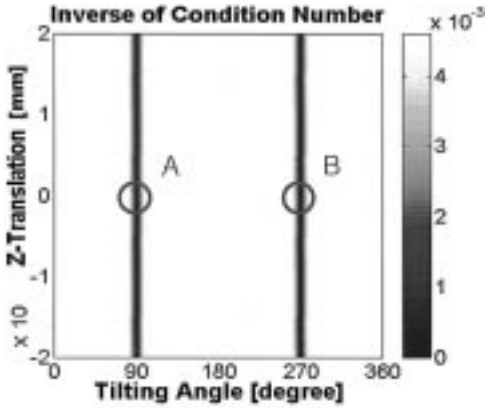


Fig. 5. Condition number plot of the end-effector singularity configuration.

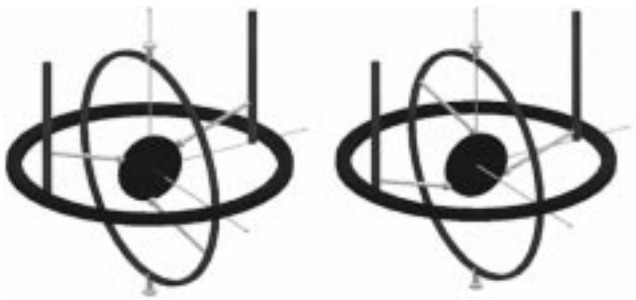

(a) (b)

Fig. 6. Examples of the end-effector singular configuration. (a) Point A in Fig. 5. (b) Point B in Fig. 5.

Finding a closed form solution for the determinant roots (singularities) of the inverse of the Jacobian is a difficult task, even when a specialized symbolic computational tool is available [12]. Besides this, once the roots have been identified, a different and even more challenging task is establishing what roots are within the workspace of the mechanism, i.e., joint values are within admissible motion range and link interferences are avoided. Another possibility for identifying the singularities of a parallel mechanism lies in the use of line geometry and screw theory [13], which is particularly suited for symmetric parallel platforms connected by six serial structures, in which the number of actuators is equal to the kinematic degrees of freedom of the platform. A different method, usually considered to be the simplest in the parallel mechanism literature, is to use a brute force algorithm and employ a numerical method that computes the condition number of the Jacobian at all points in the workspace. The condition number of $J$ is defined as the ratio of the maximum singular value to the minimum singular value.

The results in Fig. 5 are based on this numerical method, and illustrate the condition number of the forward Jacobian, while Eclipse II tilts from $0^\circ$ to $360^\circ$. The $x$ and $y$ axes in Fig. 5 represent the tilting angle and translation along the $z$ axis in the fixed frame, respectively. The dark regions around $90^\circ$ and $270^\circ$ in Fig. 5 represent the singular configurations of $J$, which are, in effect, the end-effector singularities.

Fig. 6 shows two examples of the end-effector singular configurations of the Eclipse II. The end-effector singular configurations occur in positions where, with the platform tilted at $90^\circ$ or $270^\circ$, one of the spherical joints is located on the $z$ axis of the fixed frame. If the platform reaches one of the end-effector singular configurations of the Eclipse II, there exist infinite solutions for the inverse kinematics. This also means that there exist infinite possible sets of active joint values for one specific end-effector configuration of the moving platform. Even if it is possible to select only one solution of the inverse kinematics while

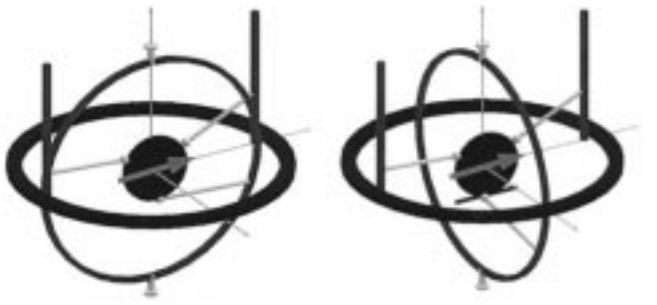

(a) (b)

Fig. 7. $y$-direction motion of the Eclipse II. (a) 6 degrees of freedom Eclipse II. (b) 6+1 degrees of freedom Eclipse II.

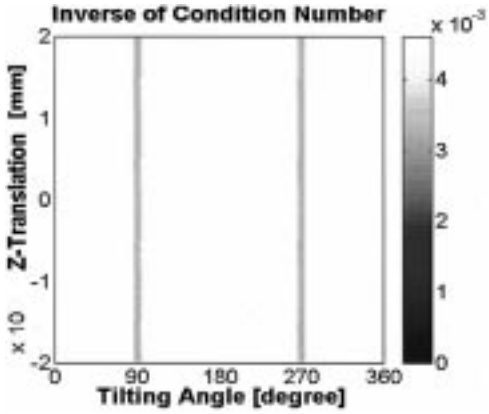


Fig. 8. Condition number plot of the end-effector singularity configuration of the 6+1 degrees of freedom Eclipse II.

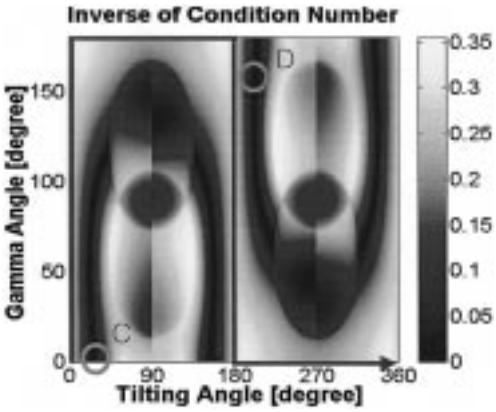


Fig. 9. Condition number plot of the actuator singularity configuration.

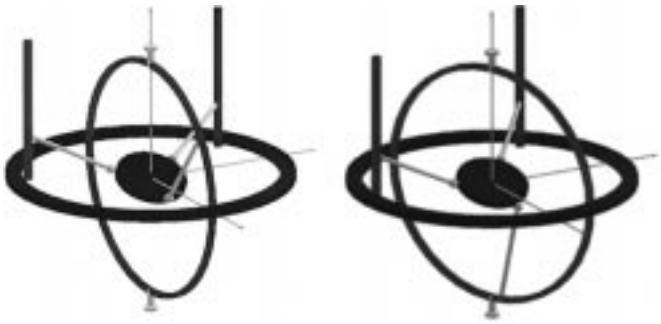

(a) (b)

Fig. 10. Examples of the actuator singular configurations. (a) Point C in Fig. 9. (b) Point D in Fig. 9.

the platform tilts from 0° to 360°, either the joints have infinite velocity or one linear column and the circular column collide with each other. As a solution to this problem, it is possible to change the solution of the inverse kinematics at the end-effector singular configuration.

However, there still remains a problem, as shown in Fig. 7(a). At this configuration, the platform cannot translate along the $y$ direction in the moving frame. Hence, an actuator is added to change the position of the spherical joint connected to the circular column, that is, one degree of freedom is added to the original Eclipse II. With this addition, the platform can now move along the $y$ direction at an end-effector singular configuration by changing the position of the spherical joint along the linear guide, whereas it is not necessary for the circular column to move [see Fig. 7(b)]. The additional actuator results in the elimination of the end-effector singularity within the workspace of the mechanism. Fig. 8 shows that the condition number of the forward kinematics Jacobian (now $J \in R^{6\times 10}$) of Eclipse II with the extra degree of freedom reduces significantly from that corresponding to Fig. 5 at the tilting angles of 90° and 270°.

### *B. Actuator Singularity*

At an actuator singularity, the mechanism gains one or more degrees of freedom of possible motion, i.e., a self-motion occurs. Actuator singularity configurations can be determined from the Jacobian of the constraint equations. In the case of the Eclipse II, the Jacobian of the constraint equation can be found by differentiating the constraint equation (7)

$$\frac{\partial g}{\partial \theta_a}\,\dot{\theta}_a + \frac{\partial g}{\partial \theta_p}\,\dot{\theta}_p = 0 \tag{12}$$

where $\partial g/\partial \theta_p$ is a $3 \times 3$ matrix.

If the matrix $\partial g/\partial \theta_p$ is not of full rank, the passive joint values cannot be determined by the given active joint values, and then the mechanism is in one of the actuator singularity configurations. Like the end-effector singularities, actuator singularities are established from the condition number of the Jacobian of the constraint equations at all points in the workspace. Fig. 9 illustrates the condition number of $\partial g/\partial \theta_p$, while the platform tilts from 0° to 360°. The $x$ axis represents the tilting angle, and the $y$ axis represents the rotation angle $\gamma$ about the $z$ axis of the moving frame. As the condition number becomes larger, the mechanism moves nearer to an actuator singular configuration. For example, in the case of $\gamma = 0$, actuator singularities occur around tilting angles of 25° and 155°, the dark regions right above the tilting angle axis in the left side of Fig. 9.

Fig. 10 shows two examples (points C and D in Fig. 9) of actuator singular configurations of the Eclipse II. In actuator singular configurations, two major problems exist. First, the platform cannot sustain its static equilibrium position in the presence of external force. In this case, the platform seems to have extra degrees of freedom. Second, the forward kinematic solutions are divided into two or more directions. Along the path crossing the actuator singular configuration, there exist multiple forward kinematic solutions with the same active joint values. Hence, there is a chance that the platform moves along an undesired direction.

One method for eliminating the actuator singular configurations is to redundantly actuate the mechanism by adding an actuator to one or more of the passive joints. In the case of Eclipse II, an additional actuator is added to one revolute joint on one of the linear columns (thus $\partial g/\partial \theta_p$ reduces to a $3 \times 2$ matrix). Choosing one of the linear columns over the other one would only imply an upside down turn of the figure. Comparing Fig. 11 with Fig. 9, it may be noted that the

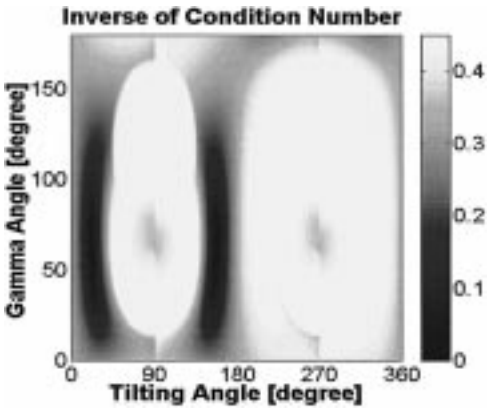


Fig. 11. Condition number plot of the actuator singularity configuration in the redundant case.

condition numbers reduced significantly, and all of the actuator singular configurations are eliminated.

## IV. Workspace Analysis

The workspace of a mechanism is defined to be the set of all positions and orientations reachable by the moving platform. The workspace analysis of the Eclipse II begins with a description of the moving frame orientation. Many parameterizations exist for describing orientation, e.g., Euler angles, fixed angles, exponential coordinates, etc. Due to the particular architecture of the Eclipse II, we choose to describe the orientation of the mechanism using the $z$-$y$-$z$ fixed angles. In terms of these, the rotation matrix is given by

$$R = \mathrm{Rot}_Z(\alpha)\mathrm{Rot}_Y(\beta)\mathrm{Rot}_Z(\gamma) \tag{13}$$

where $\alpha$, $\beta$, and $\gamma$ are the rotation angles, in succession, about the $z$, $y$, and $z$ axes of the fixed frame. When the orientation of the moving platform is described as above, the characteristic of the Eclipse II mechanism is that the tilting angle $\beta$ can reach $360^\circ$.

The actual Cartesian workspace is restricted by the following physical constraints on the mechanism:

1) stroke limit of the linear prismatic joints;
2) interference between the vertical or circular columns;
3) interference between the columns and rods;
4) rotation limit of the spherical joints.

Figs. 12 and 13 display the workspace of the Eclipse II mechanism. The rotational limits of the spherical joints are assumed to be $\pm 55^\circ$, and the two rotational angles, $\alpha$ and $\beta$, can reach $360^\circ$.

The kinematic parameters in Fig. 12 are the same as described in Section III. The workspace has cylindrical shape, with the radius and height of 90 and 340 mm, respectively. For fixed radius of the circular guide and vertical column, the enlarged workspace of the mechanism is presented in Fig. 13. For this last case, the spherical joints of the platform are placed at the apexes of an isosceles triangle, while for the original situation the ball-and-socket joints connect the apexes of an equilateral triangle. The lengths of the base and height of the isosceles triangle are 680 and 570 mm, respectively. The other kinematic parameters are the radius of circular guide and circular column, 1000 mm, and the length of the link in the circular column and of the links in the linear column, 700 and 840 mm, respectively. By simply modifying the shape of the moving platform and the lengths of the connecting links, the enlarged radius and height of the workspace increase to 170 and 520 mm, respectively.

Fig. 12. Original workspace of the Eclipse II mechanism.

Fig. 13. Enlarged workspace of the Eclipse II mechanism.

## V. Conclusions

This paper has presented a new parallel mechanism, the Eclipse II. The unique feature of the Eclipse II is that continuous $360^\circ$ rotational motion of the platform is possible, in addition to translational motion. Results of the kinematic analysis for the forward and inverse kinematics, the singular configuration, and workspace have been described. The original Eclipse II mechanism shows both end-effector and actuator singular configurations within its workspace. Hence, a linear guide, where one spherical joint moves, is added to the mechanism to eliminate the end-effector singularity. An actuator is also added to one of two passive revolute joints on the vertical columns to eliminate the actuator singularities. Therefore, the final Eclipse II is a redundantly actuated six + one-degrees- of-freedom parallel mechanism. Currently, a working sample is being built at Seoul National University, Seoul, Korea. Preliminary calculations indicate a maximum velocity of the platform of 12 m/min. and an acceleration of 0.1 g.

## References

[1] D. Stewart, "A platform with six degrees of freedom," in *Proc. Inst. Mech. Eng.*, vol. 180, 1966, pp. 371–386.
[2] J. S. Freeman, *et al.*, "The Iowa driving simulator: An implementation and application overview,", SAE Paper 950 174, 1995.
[3] G. P. Bertollini, *et al.*, "The general motors driving simulator,", SAE Paper 940 179, 1994.
[4] J.-P. Merlet, *Parallel Robots*. Amsterdam, The Netherlands: Kluwer, 2000.
[5] R. Clavel, "Conception d'un robot paralléle rapide à 4 degrés de liberté," Ph.D. dissertation, no. 925, EPFL, Lausanne, Switzerland, 1991.
[6] C. M. Gosselin and E. St-Pierre, "Development and experimentation of a fast 3-DOF camera-orienting device," *Int. J. Robot. Res.*, vol. 16, no. 5, pp. 619–630, Oct. 1997.
[7] J. M. Wiitala and M. M. Stanišić, "Design of an overconstrained and dextrous spherical wrist," *ASME J. Mech. Des.*, vol. 122, pp. 347–353, Sept. 2000.
[8] J. Kim, F. C. Park, S. Ryu, J. Kim, J. C. Hwang, C. Park, and C. Iurascu, "Design and analysis of a redundantly actuated parallel mechanism for rapid machining," *IEEE Trans. Robot. Automat.*, vol. 17, pp. 423–434, Aug. 2001.
[9] W. H. Press, S. A. Teukolsky, W. T. Vetterling, and B. F. Flannery, *Numerical Recipes in C: The Art of Scientific Computing*, 2nd ed. Cambridge, U.K.: Cambridge Univ. Press, 1995, ch. 9.

[10] The MathWorks Inc. , "Optimization Toolbox User's Guide,", Natick, MA, 1993.
[11] F. C. Park and J. W. Kim, "Singularity analysis of closed kinematic chains," *ASME J. Mech. Des.*, vol. 121, pp. 32–38, 1999.
[12] St.-O. B. Mayer and C. M. Gosselin, "Singularity analysis and representation of spatial six DOF parallel mechanisms," in *Recent Advances in Robot Kinematics*, J. Lenarčič and V. Parenti-Castelli, Eds. Amsterdam, The Netherlands: Kluwer, 1996, pp. 389–398.
[13] J.-P. Merlet, "Singular configurations of parallel manipulators and Grassmann geometry," *Int. J. Robot. Res.*, vol. 8, no. 5, pp. 45–56, Oct. 1989.

# Adaptive SP-D Control of a Robotic Manipulator in the Presence of Modeling Error in a Gravity Regressor Matrix: Theory and Experiment

H. Yazarel, C. C. Cheah, and H. C. Liaw

***Abstract*—Many controllers have been developed for setpoint control of robotic manipulators. An adaptive proportional and derivative (PD) controller is one of the simplest and most effective setpoint controller in the presence of uncertainty in gravitational force. However, an exact model of gravity regressor is required in the adaptive PD control. In this paper, we propose an adaptive setpoint controller with modeling error in the gravity regressor and show that convergence can be guaranteed even when the gravity regressor is uncertain. A new Lyapunov function is presented for stability analysis of such problem. As a byproduct of the result, we also show that existing setpoint controllers such as an adaptive saturated proportional-derivative (SP-D) and saturated proportional-integral and derivative (SP-ID) in the literature can be analyzed and designed in a unifying way as special cases of the proposed controller.**

***Index Terms*—Adaptive control, setpoint control, stability, uncertain gravity regressor.**

## I. Introduction

Since robotic manipulators have many serially linked components, the manipulator dynamics are highly nonlinear with strong couplings existing between joints. Takegaki and Arimoto [1] prove that, a simple PD (proportional and derivative) controller with gravity compensation is effective for setpoint positioning of the nonlinear mechanical systems. In the paper [1], Lyapunov stability theory is applied to robot control for the first time. Later, theoretical and experimental analysis with extensions of this type is reported [2]–[4].

In PD control [1], the exact gravitational force is assumed to be known. In practice, it is difficult to obtain the exact gravitational force. To overcome this problem, proportional, integral and derivative (PID) and adaptive PD controllers are proposed. By adding an integrator to the PD control law, a PID controller is introduced and stability is shown in a local sense [5]. Later, Arimoto [6], [7] propose a saturated proportional-integral and derivative (SP-ID) controller which gives rise to global asymptotic stability of the robot's motion. The importance of these developments [5]–[7] is that offset errors due to unknown gravity are eliminated. Though the PID controller [5]–[7] is a model-free approach that does not require any knowledge of the gravitational force, a disadvantage is that the controller may cause a large overshoot in the transient response. This is due to the fact that the error in estimating the gravitational force is large at the beginning without using any knowledge of the gravitational force.

If the structure of the gravitational force is available, adaptive setpoint controllers [7]–[16] can be used to compensate the gravitational force with better transient performance. This is because the initial error in estimating the gravitational force can be reduced by using partial knowledge of the gravitational force in the form of a gravity regressor.

In the previously proposed adaptive PD controllers [7]–[16], the exact model of gravity regressor matrix is needed. However, no model could be obtained exactly and the model could change according to different tasks. In this paper, we propose an adaptive saturated proportional-derivative (SP-D) control law with uncertain gravity regressor and prove its asymptotic convergence. A new Lyapunov function is presented for analysis of setpoint control problem with uncertain regressor. As a byproduct of the result, we shall also show that the setpoint controllers, such as adaptive SP-D and SP-ID [7] in the literature, can be analyzed and designed in a unifying way as special cases of our proposed controller. Sufficient conditions for the bound of an uncertain gravity regressor matrix and proportional and derivative gains are presented to guarantee the convergence. Simulation and experimental results are presented to illustrate the performance of the proposed controller.

## II. Problem Formulation

The equation of motion for the robotic manipulator with $n$ degrees of freedom is given in joint space as [7]

$$M(q)\ddot{q} + \left(B_0 + \frac{1}{2}\dot{M}(q) + S\left(q,\dot{q}\right)\right)\dot{q} + g(q) = \tau \tag{1}$$

where $q \in R^n$ denotes joint angles, $M(q) \in R^{n\times n}$ denotes inertia matrix which is positive definite and symmetric, $B_0 \in R^{n\times n}$ denotes a diagonal viscous friction matrix, $g(q) = (\partial P(q)/\partial q)^T \in R^n$ denotes gravitational force, $P(q)$ is the potential energy due to gravitational force, $\tau \in R^n$ denotes control inputs, and $S(q,\dot{q})$ is a skew-symmetric matrix expressed by

$$S\left(q,\dot{q}\right)\dot{q} = \frac{1}{2}\dot{M}(q)\dot{q} - \frac{1}{2}\left\{\frac{\partial}{\partial q}\dot{q}^T M(q)\dot{q}\right\}^T. \tag{2}$$

The gravitational force can be completely characterized by a set of parameters $\varphi = (\varphi_1,\ldots,\varphi_p)^T$ [7], [11], [17]–[20] as

$$g(q) = Z(q)\varphi \tag{3}$$

where $Z(q) \in R^{n\times p}$ is the gravity regressor.

In the presence of modeling error, $Z(q)$ is uncertain and we could only obtain an approximated model as $\hat{Z}(q)$. Then the control input is proposed as

$$\tau = -K_p s(e) - K_v\dot{q} + \hat{Z}\left(q_d\right)\hat{\theta} \tag{4}$$

$$\dot{\hat{\theta}} = -L\hat{Z}\left(q_d\right)^T\left(\dot{q} + \alpha s(e)\right) \tag{5}$$

where $\hat{Z}(q_d)$ is a desired gravity regressor, $e = q - q_d = (e_1,\ldots,e_n)^T$ is the positional deviation from the desired position $q_d \in R^n$, $K_p$ and $K_v$ are positive definite diagonal feedback gains for the position and velocity respectively, $L \in R^{p\times p}$ is a positive definite diagonal matrix, $\alpha$ is a positive constant, $s(e) = (s_1(e_1),\ldots,s_n(e_n))^T$, $s_i(\cdot), i = 1,\ldots,n$ are saturated functions to be defined later, and the initial estimation of $\hat{\theta}$ at $t = 0$ is chosen to be zero without loss of generality.

Manuscript received September 28, 2001; revised January 17, 2002. This paper was recommended for publication by Associate Editor S. Chiaverini and Editor I. Walker upon evaluation of the reviewers' comments.

H. Yazarel and C. C. Cheah are with the School of Electrical and Electronic Engineering, Nanyang Technological University, Singapore 639798.

H. C. Liaw is with the Gintic Institute of Manufacturing Technology, Singapore 638075.

Publisher Item Identifier S 1042-296X(02)06336-X.